The Astrophysical Journal Letters, 738:L32 (6pp), 2011 September 10 doi:10.1088/2041-8205/738/2/L32

r-PROCESS NUCLEOSYNTHESIS IN DYNAMICALLY EJECTED MATTER OF NEUTRON STAR MERGERS

Stephane Goriely[1], Andreas Bauswein[2], and Hans-Thomas Janka[2]
[1] Institut d'Astronomie et d'Astrophysique, Université Libre de Bruxelles, C.P. 226, B-1050 Brussels, Belgium
[2] Max-Planck-Institut für Astrophysik, Postfach 1317, D-85741 Garching, Germany
Received 2011 July 5; accepted 2011 August 9; published 2011 August 24

ABSTRACT

Although the rapid neutron-capture process, or *r*-process, is fundamentally important for explaining the origin of approximately half of the stable nuclei with $A > 60$, the astrophysical site of this process has not been identified yet. Here we study *r*-process nucleosynthesis in material that is dynamically ejected by tidal and pressure forces during the merging of binary neutron stars (NSs) and within milliseconds afterward. For the first time we make use of relativistic hydrodynamical simulations of such events, defining consistently the conditions that determine the nucleosynthesis, i.e., neutron enrichment, entropy, early density evolution and thus expansion timescale, and ejecta mass. We find that 10^{-3}–10^{-2} $M_\odot$ are ejected, which is enough for mergers to be the main source of heavy ($A \gtrsim 140$) galactic *r*-nuclei for merger rates of some 10^{-5} yr^{-1}. While asymmetric mergers eject 2–3 times more mass than symmetric ones, the exact amount depends weakly on whether the NSs have radii of ∼15 km for a "stiff" nuclear equation of state (EOS) or ∼12 km for a "soft" EOS. *r*-process nucleosynthesis during the decompression becomes largely insensitive to the detailed conditions because of efficient fission recycling, producing a composition that closely follows the solar *r*-abundance distribution for nuclei with mass numbers $A > 140$. Estimating the light curve powered by the radioactive decay heating of *r*-process nuclei with an approximative model, we expect high emission in the *B*-*V*-*R* bands for 1–2 days with potentially observable longer duration in the case of asymmetric mergers because of the larger ejecta mass.

Key words: nuclear reactions, nucleosynthesis, abundances – stars: abundances – stars: neutron

Online-only material: color figures

1. INTRODUCTION

The *r*-process, or rapid neutron-capture process, of stellar nucleosynthesis is invoked to explain the production of the stable (and some long-lived radioactive) neutron-rich nuclides heavier than iron, which are observed in stars of different metallicities as well as in the solar system (for a review see Arnould et al. 2007). Despite a growing wealth of observational data (e.g., Sneden et al. 2008), and although increasingly better *r*-process models with new astrophysical or nuclear physics ingredients have been developed over the decades, the stellar production site(s) of *r*-process material has (have) not been identified yet. All proposed scenarios face serious problems. Supernovae (SNe), for example, appear attractive because of their potential to explain observational features of the galactic chemical enrichment history (e.g., Argast et al. 2004). Their nucleosynthesis, however, exhibits extreme sensitivity to the detailed conditions in the ejecta, whose viability for strong *r*-processing could not be verified by sophisticated hydrodynamical models (e.g., Hoffman et al. 2008; Janka et al. 2008; Roberts et al. 2010; Hüdepohl et al. 2010; Fischer et al. 2010; Wanajo et al. 2011).

Early in the development of the theory of nucleosynthesis, an alternative origin of *r*-process nuclei was proposed (Tsuruta & Cameron 1965). It relies on the fact that at high densities (typically $\rho > 10^{10}$ g cm^{-3}) matter tends to be composed of nuclei lying on the neutron-rich side of the valley of nuclear stability as a result of endothermic free-electron captures. The astrophysical plausibility of this production mechanism as the source of the observed *r*-nuclides has long been questioned. It remained largely unexplored until Lattimer et al. (1977) and Meyer (1989) studied the decompression of cold, neutronized matter ejected by tidal effects of a black hole (BH) on a neutron star (NS) companion. Recently, special attention has been paid to NS mergers because hydrodynamic simulations of NS–NS and NS–BH mergers showed that a non-negligible amount of matter may be ejected (e.g., Janka et al. 1999; Rosswog et al. 2004; Oechslin et al. 2007).

All previous investigations of the ejecta from coalescing NSs (Freiburghaus et al. 1999; Goriely et al. 2005; Arnould et al. 2007; Metzger et al. 2010; Roberts et al. 2011) were parameterized in one way or another, which makes their results and conclusions subject to open questions. In Goriely et al. (2005) and Arnould et al. (2007) the thermodynamic profiles were constructed by a simple decompression model (see Goriely et al. 2011), but the neutron enrichment (or equivalently the electron fraction Y_e) was consistently taken from β-equilibrium assumed to have been achieved at the initial density prior to the decompression. It was found that the final composition of the material ejected from the inner crust depends on the initial density, at least for the outer parts of the inner crust at $\rho_{\rm drip} \leqslant \rho \leqslant 10^{12}$ g cm^{-3} (where $\rho_{\rm drip} \simeq 4.2 \times 10^{11}$ g cm^{-3}, is the neutron-drip density). For the deeper inner-crust layers ($\rho > 10^{12}$ g cm^{-3}), large neutron-to-seed ratios drive the nuclear flow into the very heavy mass region, leading to multiple fission recycling. As a consequence, the resulting abundance distribution becomes independent of the initial conditions, especially of the initial density. It was found to be in close agreement with the solar distribution for $A > 140$ nuclei (Goriely et al. 2005; Arnould et al. 2007).

Different approaches were taken to nucleosynthesis calculations for merger ejecta by Freiburghaus et al. (1999), Metzger et al. (2010), and Roberts et al. (2011). In their calculations, while the density evolution of the mass elements was adopted from hydrodynamical simulations, both the initial neutron enrichment and the temperature history were considered as free

parameters. In particular, Y_e was chosen in order to obtain, after decompression, an *r*-abundance distribution as close as possible to the solar distribution. This led to values of $Y_e = 0.1$ (Freiburghaus et al. 1999) or 0.2 (Roberts et al. 2011), corresponding to relatively near-surface layers of the inner crust and to nuclear flows that are not subject to multiple fission cycles. In our simulations, most of the ejecta mass originates from the deep layers of the inner crust so that any contribution from near-surface layers remains minor. In addition, previous studies assumed that the nucleosynthesis is independent of the initial temperature of the ejected material, while we find that the initial temperature may not only affect the initial composition, but potentially also the nucleosynthesis (see Section 3) so that special attention should be paid to the detailed temperature history of the ejected material prior to its free expansion.

The work presented here is based on recent three-dimensional relativistic simulations of NS–NS mergers to determine the nucleosynthesis-relevant conditions of the ejected matter. The hydrodynamical model is described in Section 2. Section 3 presents the nucleosynthesis results for two binaries, a symmetric NS–NS system and an asymmetric one. In contrast to previous studies, detailed information about the density, Y_e, and entropy evolution of the ejecta is extracted from the hydrodynamical simulations and included in the network calculations. The expected electromagnetic emission that is powered by radioactive decays following the heavy-element nucleosynthesis is estimated by a simple, approximative light-curve model in Section 4. Conclusions are drawn in Section 5.

2. HYDRODYNAMICAL MODELS

Our NS–NS merger simulations were performed with a general relativistic smoothed particle hydrodynamics scheme (Oechslin et al. 2007; Bauswein et al. 2010) representing the fluid by a set of particles with constant rest mass, whose hydrodynamical properties were evolved according to Lagrangian hydrodynamics, keeping Y_e of fluid elements fixed. The Einstein field equations were solved assuming a conformally flat spatial metric. Binaries with two mass ratios were modeled, namely symmetric 1.35–1.35 $M_\odot$ and asymmetric 1.2–1.5 $M_\odot$ systems, both with a resolution of about 550,000 particles. The 1.35–1.35 $M_\odot$ case is of particular interest since, according to population synthesis studies and pulsar observations, it represents the most abundant systems (Belczynski et al. 2008).

For the results presented here we used the Shen et al. (1998) equation of state (EOS), which includes thermal effects that become important when the NSs collide. The corresponding NSs have radii of ∼15 km (see Bauswein et al. 2010). To assess the EOS influence on gross properties of the ejecta, we also performed simulations with the Lattimer & Swesty (1991) LS220 EOS with an incompressibility modulus of 220 MeV and a NS radius of ∼12 km. Note that both of our EOSs are in agreement with the observation of a 2 $M_\odot$ NS (Demorest et al. 2010). Since an accurate calculation of the temperature evolution in the hydrodynamic simulations is hampered by high initial degeneracy and limited numerical resolution, we postprocessed the temperature of each ejected fluid element by assuming an adiabatic flow in the absence of shocks and increasing the specific entropy (consistent with the shock-jump conditions) when a shock was detected.

In the case of the symmetric NS binary, about 3×10^{-3} $M_\odot$ are found to become gravitationally unbound, whereas about 6×10^{-3} $M_\odot$ are ejected from the asymmetric system (using the LS220 EOS, we obtain an ejecta mass of $\sim 2 \times 10^{-3}$ $M_\odot$ and 6×10^{-3} $M_\odot$, respectively). The ejected "particles" (i.e., mass elements) originate mostly from two different regions in the inner crust of the initial stars. For the symmetric model, ∼75% of the material are squeezed out from the contact interface of the NSs. The remaining 25% are ejected from the near-surface regions close to the orbital plane, see inset of Figure 1, where the arrows indicate by trend which initial densities the majority of fluid elements corresponds to. Note that the "contact" interface of the asymmetric merger is different from the symmetric case. While in the latter the two NSs collide in a shearing way and violently along a broad area, the impact of the tidally stretched lower-mass companion in the asymmetric case happens in a more grazing way such that a conical "nose" of the lower-mass star digs off matter from the higher-mass object. For this reason, in the asymmetric system the contact region preferentially contributes to ejecta with low initial densities. As seen in Figure 1, all ejecta have low Y_e ranging between 0.015 and 0.050 (about 30% of the mass have $Y_e \sim 0.015$). In the asymmetric case a small amount of ejected material starts out from densities above 2×10^{14} g cm^{-3} and has Y_e-values up to 0.07. For the first 27 ms, the density history is consistently followed by the numerical simulation. Afterward, the escaping ejecta are assumed to expand freely with constant velocity. The radii of the ejecta clumps thus grow linearly with time t and consequently their densities drop like $1/t^3$. Note that due to a lack of resolution the dynamics and mass of unbound crust material with initial densities $\rho \lesssim 10^{13}$ g cm^{-3} cannot be reliably calculated in the hydrodynamic model. However, compared to the 10^{-3}–10^{-2} $M_\odot$ of inner crust matter its contribution to the ejecta remains small.

The ejected matter is initially cold, but most of it gets shock-heated during the ejection to temperatures above 1 MeV. Its composition is then determined by nuclear statistical equilibrium (NSE). When the drip density is reached during expansion, most of the matter has cooled to below 1 MeV and the NSE composition has frozen out. As soon as the temperature has dropped below 10^{10} K, further changes of the composition are followed by a full network calculation (as detailed below), and the temperature evolution is determined on the basis of the laws of thermodynamics, allowing for possible nuclear heating through β-decays, fission, and α-decays, as described in Meyer (1989).

3. NUCLEOSYNTHESIS

The reaction network includes all 5000 species from protons up to $Z = 110$ lying between the valley of β-stability and the neutron-drip line. All fusion reactions on light elements that play a role when the NSE freezes out are included in addition to radiative neutron captures and photodisintegrations. The reaction rates on light species are taken from the NETGEN library, which includes all the latest compilations of experimentally determined reaction rates (Xu et al. 2011). Experimentally unknown reactions are estimated with the TALYS code (Goriely et al. 2008) on the basis of the HFB-21 nuclear mass model (Goriely et al. 2010). On top of these reactions, fission and β-decays are also included, i.e., neutron-induced fission, spontaneous fission, β-delayed fission, photofission, as well as β-delayed neutron emission. The β-decay processes are taken from the updated version of the Gross Theory (Tachibana et al. 1990) based on the HFB-14 Q-values, whereas all fission processes are estimated on the basis of the HFB-14 fission path and the full calculation of the corresponding barrier penetration (Goriely

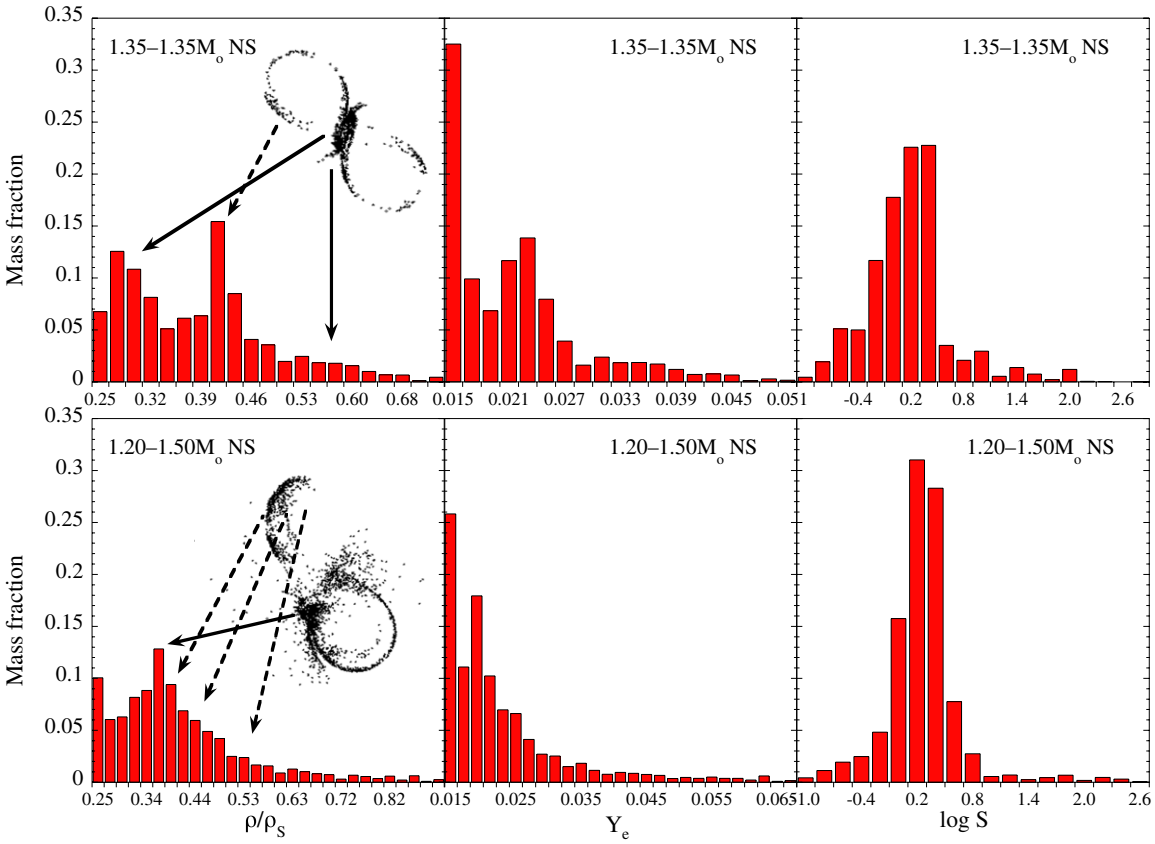

Figure 1. Histograms of fractional mass distribution of the ejecta for the 1.35–1.35 $M_\odot$ NS merger (upper row) and the 1.2–1.5 $M_\odot$ binary (lower row) as functions of density ρ (relative to the saturation density $\rho_S \simeq 2.6 \times 10^{14}$ g cm^{-3}; left) and of electron fraction Y_e (middle) that the ejected matter had at its initial NS location prior to merging. The right panels show the fractional mass distributions as functions of the final entropy S per nucleon when the matter starts its free expansion. In the inset on the left panels the dots mark positions of mass elements that get ejected later. The locations are given in the projection on the orbital plane at the time when the stellar collision begins.

(A color version of this figure is available in the online journal.)

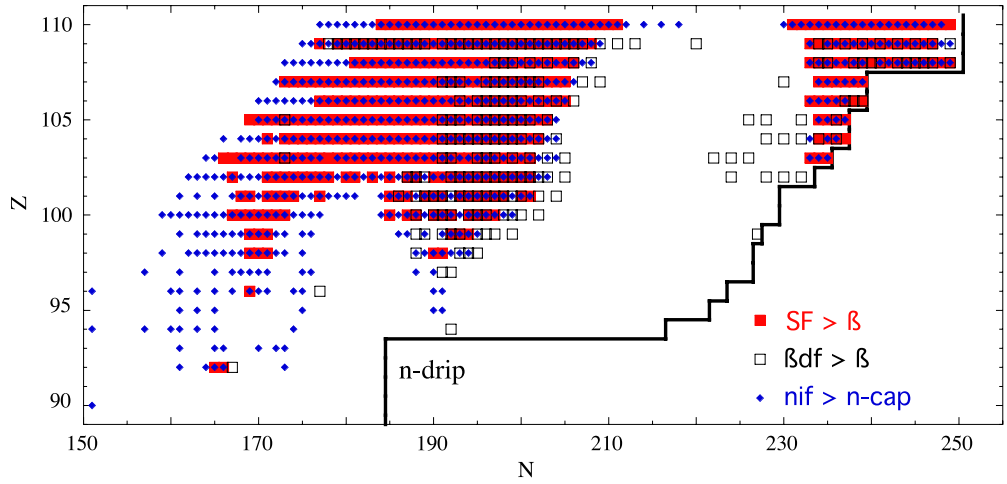

Figure 2. Representation of dominant fission regions in the (N, Z) plane. Nuclei for which spontaneous fission is estimated to be faster than β-decays are shown by full squares, those for which β-delayed fission is faster than β-decays by open squares, and those for which neutron-induced fission is faster than radiative neutron capture at $T = 10^9$ K by diamonds.

(A color version of this figure is available in the online journal.)

et al. 2009). The main fission region is illustrated in Figure 2. The fission fragment distribution is taken from Kodoma & Takahashi (1975), and the fragment mass and charge asymmetry are derived from the HFB-14 prediction of the left–right asymmetry at the outer saddle point. Due to the specific initial conditions of high neutron densities (typically $N_n \simeq 10^{33}$–10^{35} cm^{-3} at the drip density), the nuclear flow during most of the neutron irradiation will follow the neutron-drip line. For these nuclei at $T \gtrsim 2$–3×10^9 K, $(n, 2n)$ and $(2n, n)$ reactions are faster than (γ,n) and (n,γ) reactions and must be included in the reaction network. The $(n, 2n)$ rates are estimated with the TALYS code and the reverse rates from detailed balance expressions.

For drip-line nuclei with $Z \geqslant 103$, fission becomes efficient (Figure 2) and recycling takes place two to three times before

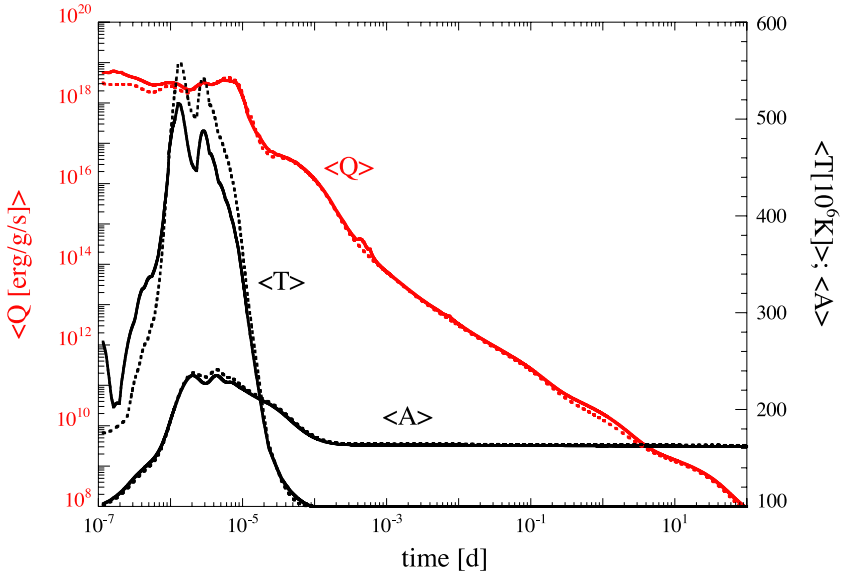

Figure 3. Time evolution of the total radioactive heating rate per unit mass, $\langle Q \rangle$, mass number $\langle A \rangle$, and temperature $\langle T \rangle$ (all mass-averaged over the ejecta) for the 1.35–1.35 $M_\odot$ (solid lines) and 1.2–1.5 $M_\odot$ (dotted lines) NS mergers.

(A color version of this figure is available in the online journal.)

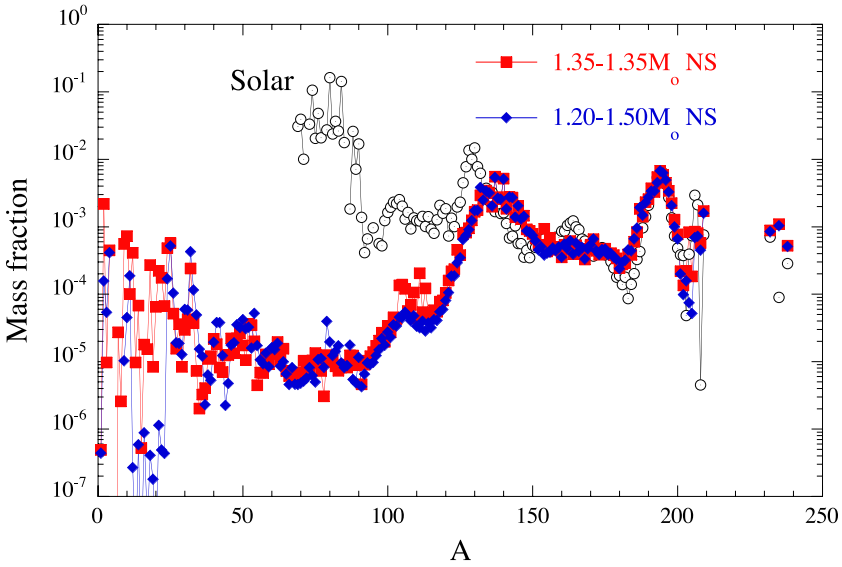

Figure 4. Final nuclear abundance distributions of the ejecta from 1.35–1.35 $M_\odot$ (squares) and 1.2–1.5 $M_\odot$ (diamonds) NS mergers as functions of atomic mass. The distributions are normalized to the solar *r*-abundance distribution (dotted circles).

(A color version of this figure is available in the online journal.)

the neutrons are exhausted, as shown in Figure 3 by the time evolution of the mass number $\langle A \rangle$ mass-averaged over all the ejecta. After several hundred ms, when neutrons get exhausted by captures ($N_n \sim 10^{20}$ cm^{-3}), n-captures and β-decays compete on similar timescales and fashion the final abundance pattern before the nuclear flow becomes dominated by β-decays (as well as fission and α-decays for the heaviest species) back to the stability line. The average temperature remains rather low during the late neutron irradiation, around 0.5 GK (Figure 3), so that photoreactions do not play a major role.

The final mass-integrated ejecta composition is shown in Figure 4. The $A = 195$ abundance peak related to the $N = 126$ shell closure is produced in solar distribution and found to be almost insensitive to all input parameters such as the initial abundances, the expansion timescales, and the adopted nuclear models. In contrast, the peak around $A = 140$ originates exclusively from the fission recycling, which takes place in the $A \simeq 280$–290 region at the time all neutrons have been captured. These nuclei are predicted to fission symmetrically as visible in Figure 4 by the $A \simeq 140$ peak corresponding to the mass-symmetric fragment distribution. It is emphasized that significant uncertainties still affect the prediction of fission probabilities and fragment distributions so that the exact strength and location of the $A \simeq 140$ fission peak (as well as the possible $A = 165$ bump observed in the solar distribution) depend on the adopted nuclear model.

While most of the matter trajectories are subject to a density and temperature history leading to the nuclear flow and abundance distribution described above, some mass elements can be shock-heated at relatively low densities. Typically at $\rho > 10^{10}$ g cm^{-3}, the Coulomb effects shift the NSE abundance distribution toward the high-mass region (Goriely et al. 2011), but at lower densities, the high temperatures lead to the photodissociation of all the medium-mass seed nuclei into

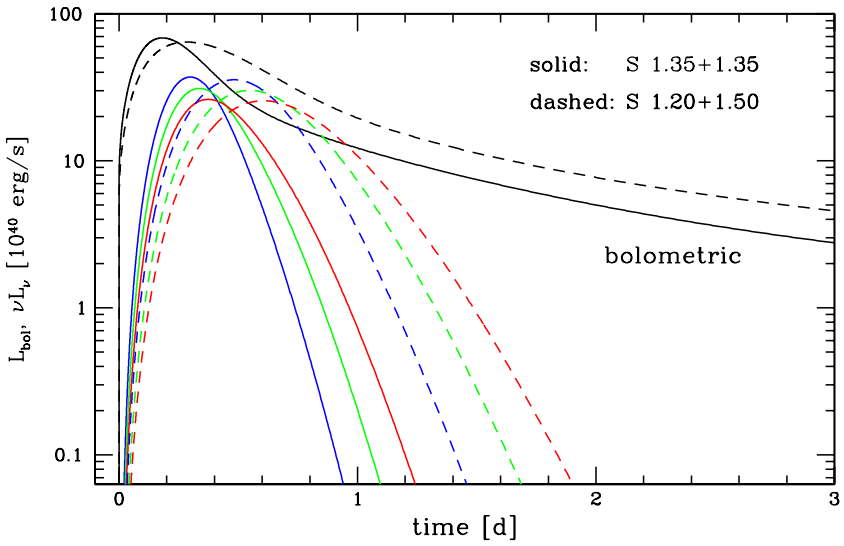

Figure 5. Photon luminosities of the expanding NS merger ejecta caused by radioactive decay heating for the 1.35–1.35 $M_\odot$ (solid lines) and 1.2–1.5 $M_\odot$ (dashed lines) binaries. The upper, long-duration lines are the bolometric luminosities, the sequences of short-duration peaks correspond to the emission in the blue, visual, and red wavebands (at wavelengths of 445, 551, 658 nm; from left to right).

(A color version of this figure is available in the online journal.)

neutrons and protons. Nucleon recombination may occur during the decompression provided the expansion timescale of the trajectories is long enough. For a non-negligible amount of ejected material, this recombination is indeed inefficient so that light species (including D and ^{4}He) are also found in the ejecta (Figure 4). The final yields of $A < 140$ nuclei remain, however, small and are not expected to contribute to any significant enrichment of the interstellar medium compared to the heavier *r*-elements.

4. ELECTROMAGNETIC COUNTERPARTS

Radioactive power through β-decays, fission processes, as well as late-time α-decays will heat the expanding ejecta and make them radiate as a "macro-nova" (Kulkarni 2005) or "kilo-nova" (Metzger et al. 2010) associated with the ejection of nucleosynthesis products from the merger (Li & Paczyński 1998). The time evolution of the corresponding total mass-averaged energy release rate available for heating the ejecta (i.e., energy escaping in neutrinos is not considered) is plotted in Figure 3 for both the 1.35–1.35 $M_\odot$ and 1.2–1.5 $M_\odot$ binaries. While $\langle Q(t)\rangle$ and the average temperature evolution differ only slightly between both NS–NS systems, the ejecta masses $M_{\rm ej}$ and mass-averaged expansion velocities $v_{\rm exp}$ differ considerably. While we find for the symmetric system $v_{\rm exp} \approx 0.31c$ (c being the speed of light) and $M_{\rm ej} \approx 3 \times 10^{-3}\,M_\odot$, corresponding to a total heating energy of $E_{\rm heat} \approx 2 \times 10^{49}$ erg or 3.4 MeV nucleon^{-1}, the numbers for the asymmetric case are $v_{\rm exp} \approx 0.23c$, $M_{\rm ej} \approx 6 \times 10^{-3}\,M_\odot$, and $E_{\rm heat} \approx 4 \times 10^{49}$ erg (again 3.4 MeV nucleon^{-1}).[3] This must be expected to lead to significant differences in the brightness evolution of the kilo-nova because its peak bolometric luminosity scales with $L_{\rm peak} \propto v_{\rm exp}^{1/2} M_{\rm ej}^{1/2}$ and, for free expansion ($v_{\rm exp}$ = const.), is reached on a timescale $t_{\rm peak} \propto v_{\rm exp}^{-1/2} M_{\rm ej}^{1/2}$ (Metzger et al. 2010; Arnett 1982).

[3] In the simulations with the LS220 EOS we obtain $v_{\rm exp} \approx 0.28c$ for the symmetric and $v_{\rm exp} \approx 0.24c$ for the asymmetric binary.

We calculate an approximation of the light curves of such events by employing a semi-analytic, simplified one-zone model of Kulkarni (2005; see also Arnett 1982; Li & Paczyński 1998), assuming that asymmetries of the emission remain modest (cf. Roberts et al. 2011). The EOS includes photons as well as nuclei and electrons, whose recombination fraction with decreasing temperature is approximated by that of ^{56}Ni (Arnaud & Rothenflug 1985). The opacity $\kappa = 0.4\,Z/A$ cm^2 g^{-1} for Thomson scattering is used, taking mass-averaged Z and A from the nucleosynthesis yields (Figure 3) and ignoring electron recombination as suggested by Roberts et al. (2011).

Our results for the bolometric light curves $L_{\rm bol}(t)$ and the *B*-, *V*-, and *R*-band luminosities $\nu L_\nu(t)$ are displayed in Figure 5. While we expect significant emission in the chosen wavelength bands up to $(\nu L_\nu)_{\rm peak} \approx 4 \times 10^{41}$ erg s^{-1} for about one day in the case of a 1.35–1.35 $M_\odot$ merger, the 1.2–1.5 $M_\odot$ system produces sizable *BVU*-radiation nearly twice as long.

5. CONCLUSIONS

Using relativistic NS merger models to determine the nucleosynthesis-relevant conditions self-consistently, we confirm that decompressed NS matter ejected dynamically during the stellar collision and shortly afterward is an extremely promising site for robust, strong *r*-processing. Matter from the inner crust of the coalescing NSs, which dominates the ejecta by far, produces an *r*-abundance distribution very similar to the solar one for nuclei with $A > 140$. Nuclei with $A < 140$ with solar distribution could originate from the outer crust (Goriely et al. 2011), but too little of such matter gets ejected to explain the solar proportion of light-to-heavy *r*-process material. However, significant amounts of $A < 140$ nuclei might be produced in the outflow of a BH-torus system formed after the NS merger (Wanajo & Janka 2011).

The underlying nuclear mechanisms differ significantly from those at action in SN scenarios. In particular, fission plays a major role in recycling heavy material. The similarity between predicted and solar abundance patterns as well as the robustness of the prediction against variations of input parameters, which we have shown in Goriely et al. (2005), have demonstrated here

in comparison of symmetric and asymmetric NS–NS mergers, and will further elaborate on in a forthcoming paper, make this site one of the most promising, deserving further exploration concerning hydrodynamics, galactic chemical evolution, nucleosynthesis, nuclear physics, and astronomical consequences.

Fully relativistic simulations including neutrino transport and magnetic fields, with good resolution of the inner (and outer) crust layers of the merging NSs assured by adaptive refinement, are needed to corroborate the ejecta conditions found in our work. With our yield of $\sim$(3–5) $\times 10^{-5}\,M_{\odot}$ per event of ^{151,153}Eu, a nearly pure *r*-process element, the origin of all galactic Eu from NS–NS mergers would require an event rate of $\sim$(2–3) $\times 10^{-5}$ yr^{-1}, fully compatible with present best estimates (see, e.g., Belczynski et al. 2008). However, also mass loss during the evolution of the merger remnant from a hypermassive NS to a massively accreting BH-torus system as well as NS–BH mergers with higher ejecta masses might add to the production (e.g., Wanajo & Janka 2011; Caballero et al. 2011) and deserve more detailed investigations. From the nuclear point of view, this site also implies new challenges because it involves the formation of neutron-drip nuclei, for which β-decay, neutron capture, and fission rates need to be determined. Astronomically, the discovery of electromagnetic radiation from kilo-nova events (Roberts et al. 2011; Metzger et al. 2010) could mean the first in situ observation of freshly produced *r*-process material.

H.-T.J. thanks M. Kromer and S. Hachinger for discussions. DFG grants SFB/TR7, SFB/TR27, and EXC 153, computing at LRZ and RZG, and support of F.N.R.S. and "Actions de recherche concertées (ARC)" from the "Communauté française de Belgique" are acknowledged.

REFERENCES

Argast, D., Samland, M., Thielemann, F.-K., & Qian, Y. 2004, A&A, 416, 997
Arnaud, M., & Rothenflug, R. 1985, A&AS, 60, 425
Arnett, W. D. 1982, ApJ, 253, 785
Arnould, M., Goriely, S., & Takahashi, K. 2007, Phys. Rep., 450, 97
Bauswein, A., Janka, H.-T., & Oechslin, R. 2010, Phys. Rev. D, 82, 084043
Belczynski, K., O'Shaughnessy, R., Kalogera, V., et al. 2008, ApJ, 680, L129
Caballero, O. L., McLaughlin, G. C., & Surman, R. 2011, ApJ, submitted (arXiv:1105.6371)
Demorest, P. B., Pennucci, T., Ransom, S. M., Roberts, M. S. E., & Hessels, J. W. T. 2010, Nature, 467, 1081
Fischer, T., Whitehouse, S. C., Mezzacappa, A., Thielemann, F.-K., & Liebendörfer, M. 2010, A&A, 517, A80
Freiburghaus, C., Rosswog, S., & Thielemann, F.-K. 1999, ApJ, 525, L121
Goriely, S., Chamel, N., Janka, H.-T., & Pearson, J. M. 2011, A&A, 531, A78
Goriely, S., Chamel, N., & Pearson, J. M. 2010, Phys. Rev. C, 82, 035804
Goriely, S., Demetriou, P., Janka, H.-T., & Pearson, J. M. 2005, Nucl. Phys. A, 758, 587
Goriely, S., Hilaire, S., & Koning, A. J. 2008, A&A, 487, 76
Goriely, S., Hilaire, S., Koning, A. J., Sin, M., & Capote, R. 2009, Phys. Rev. C, 79, 024612
Hoffman, R. D., Müller, B., & Janka, H.-T. 2008, ApJ, 676, L127
Hüdepohl, L., Müller, B., Janka, H.-T., Marek., A., & Raffelt, G. G. 2010, Phys. Rev. Lett., 104, 251101
Janka, H.-T., Eberl, T., Ruffert, M., & Fryer, C. L. 1999, ApJ, 527, L39
Janka, H.-T., Müller, B., Kitaura, F. S., & Buras, R. 2008, A&A, 485, 199
Kodoma, T., & Takahashi, K. 1975, Nucl. Phys. A, 239, 489
Kulkarni, S. R. 2005, arXiv:astro-ph/0510256
Lattimer, J. M., Mackie, F., Ravenhall, D. G., & Schramm, D. N. 1977, ApJ, 213, 225
Lattimer, J. M., & Swesty, F. D. 1991, Nucl. Phys. A, 535, 331
Li, L.-X., & Paczyński, B. 1998, ApJ, 507, L59
Metzger, B. D., Martinez-Pinedo, G., Darbha, S., et al. 2010, MNRAS, 406, 2650
Meyer, B. S. 1989, ApJ, 343, 254
Oechslin, R., Janka, H.-T., & Marek, A. 2007, A&A, 467, 395
Roberts, L. F., Kasen, D., Lee, W. H., & Ramirez-Ruiz, E. 2011, ApJ, 736, L21
Roberts, L. F., Woosley, S. E., & Hoffman, R. D. 2010, ApJ, 722, 954
Rosswog, S., Speith, R., & Wynn, G. A. 2004, MNRAS, 351, 1121
Shen, H., Toki, H., Oyamatsu, K., & Sumiyoshi, K. 1998, Nucl. Phys. A, 637, 435
Sneden, C., Cowan, J. J., & Gallino, R. 2008, ARA&A, 46, 241
Tachibana, T., Yamada, M., & Yoshida, Y. 1990, Prog. Theor. Phys., 84, 641
Tsuruta, S., & Cameron, A. G. W. 1965, Can. J. Phys., 43, 2056
Wanajo, S., & Janka, H.-Th. 2011, ApJ, submitted (arXiv:1106.6142)
Wanajo, S., Janka, H.-Th., & Müller, B. 2011, ApJ, 726, L15
Xu, Y., Takahashi, K., Goriely, S., & Arnould, M. 2011, in AIP Conf. Ser., Frontiers in Nuclear Structure, Astrophysics and Reactions, ed. P. Demetriou et al. (Melville, NY: AIP), in press (see also http://www.astro.ulb.ac.be/Netgen)